HOSTED BY
ELSEVIER
CrossMark
Available online at www.sciencedirect.com
ScienceDirect
Defence Technology 11 (2015) 85–92
www.elsevier.com/locate/dt

# Semi-analytical method for calculating aeroelastic effect of profiled rod flying at high velocity

Hui-jun NING [a,*], Nan-peng FENG [b], Tan-hui WU [c], Cheng ZHANG [a], Hao WANG [a]

[a] School of Energy and Power Engineering, Nanjing University of Science and Technology, Nanjing 210094, Jiangsu, China
[b] The Graduate School of Hubei Aerospace Technology Academe, Wuhan 430000, Hubei, China
[c] Dept. of Engineering Mechanics, Shanghai Jiaotong University, Shanghai 200240, China

Received 27 April 2014; revised 24 October 2014; accepted 24 October 2014
Available online 5 January 2015

**Abstract**

The key technique of a kinetic energy rod (KER) warhead is to control the flight attitude of rods. The rods are usually designed to different shapes. A new conceptual KER named profiled rod which has large L/D ratio is described in this paper. The elastic dynamic equations of this profiled rod flying at high velocity after detonation are set up on the basis of Euler-Bernoulli beam, and the aeroelastic deformation of profiled rod is calculated by semi-analytical method for calculating the vibration characteristics of variable cross-section beam. In addition, the aeroelastic deformation of the undeformed profiled rod and the aeroelastic deformation of deformed profiled rod which is caused by the detonation of explosive are simulated by computational fluid dynamic and finite element method (CFD/FEM), respectively. A satisfactory agreement of these two methods is obtained by the comparison of two methods. The results show that the semi-analytical method for calculating the vibration characteristics of variable cross-section beam is applied to analyze the aeroelastic deformation of profiled rod flying at high velocity.


*Keywords:* Profiled rod; Detonation process; Variable cross-section beam; Aeroelastic deformation; Numerical analysis

## 1. Introduction

The advanced technologies of kinetic energy rod (KER) warheads have been developed widely. According to the different threat targets, KER warheads are usually divided into continuous rod warhead and discrete rod warhead. The advantages of these warhead devices are the high speed and continuous cutting capacity for threat aircraft and cruise missiles [1–5].

However, the thicker components, which are internal submunition components of missiles, cannot be destroyed by traditional KER warheads in the missile-defense environment. Therefore, it is necessary and urgent for a new warhead mechanism with a strong killing effect against the key components of thick targets.

This paper describes a new conceptual profiled rod warhead which is different from the conventional KER warhead. The rods in the warhead are changed into variable cross-section straight rods with large L/D ratio, which we call profiled rods. The conventional rods are constant cross-section cylindrical rods and square rods. The profiled rod is designed to truncated cone shaped rod, as shown in Fig. 1. Since the shape of profiled rod is changed, the mass is unevenly distributed along the axial direction of the rod, and the velocity gradient or difference between the head and aft end of the rod is generated, which causes the different obliquity angles to strike a target. In this process, the rods initially rely on its high velocity to penetrate the target. Although the rod velocity decreases under the influence of the air resistance after the detonation, it can provide a better penetration angle that still maintains a high penetrability against targets when it moves

* Corresponding author.
*E-mail address:* ninghui85@163.com (H.J. NING).
Peer review under responsibility of China Ordnance Society.

http://dx.doi.org/10.1016/j.dt.2014.10.002

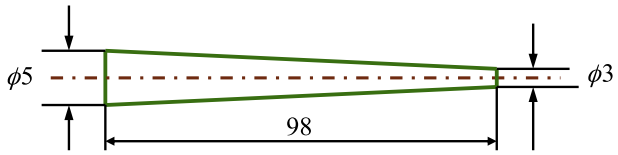


Fig. 1. Structural representation of profiled rod.

for a long range. On the other hand, the profiled rod warheads also have a continuous cutting capacity for threat aircraft and cruise missiles by setting the different angles between rods and explosive compared with the traditional KER warheads described in Refs. [6–8].

The formation of profiled rod warhead, the initial deployment velocity, the damage effect and the flight attitude of rod after detonation are analyzed in the development effort. In this paper, we focus on the latter. After the detonation, the rods obtain high deployment velocity and fly against the air resistance until they strike the target. It should be pointed out that the aeroelastic deformation of rod which is caused by overcoming the aerodynamic force at high speed has influence on flight attitude and damage effect. Consequently, an investigation on elastic deformation of profiled rod under the aerodynamic force is very important.

## 2. Design principle of profiled rod

A profiled rod with diameters of 3 mm and 5 mm, length of 98 mm and length-to-diameter ratio of 24.5 is proposed. Its model is shown in Fig. 1.

An initial motion state of the profiled rod after detonation is assumed, as shown in Fig. 2. In an analysis on the element of one end of the profiled rod, $v_0$ is the radial velocity of profiled rod, $v_r$ is the linear velocity around the $y$-axis, and $v_{c0}$ is the center of mass velocity.

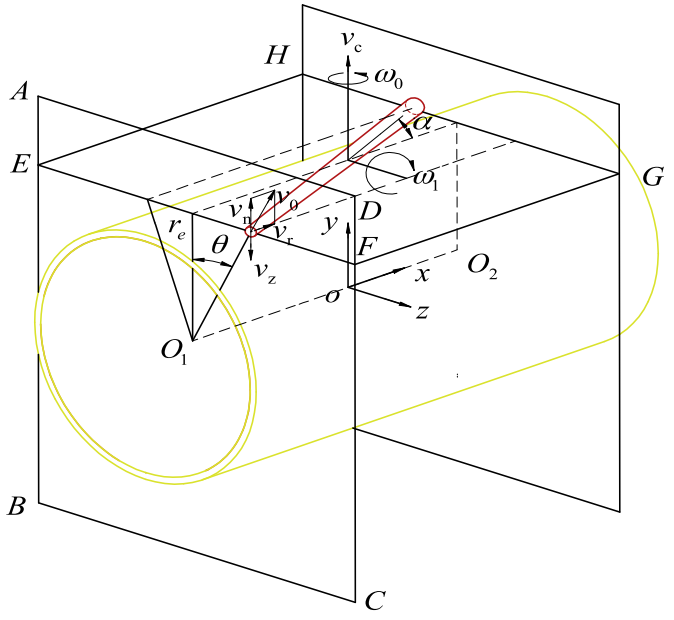


Fig. 2. Initial motion state map of a profiled rod.

Assume that $\alpha$ is the incidence angle, $L_r$ is the length of profiled rod, $\omega_0$ is the initial transverse angular velocity, $\omega_1$ is the initial turning angular velocity, and $r$ and $R$ represent the radii of the top and bottom of profiled rod, respectively. The relation between $\alpha$ and $v_r$ is deduced by

$$v_r = v_0 \sin\theta \cos\alpha \tag{1}$$

where $\theta$ is written as

$$\theta = \arctan\left(\frac{L_c}{r}\sin\alpha\right) \tag{2}$$

here,

$$L_c = L_r\left[1 - \frac{R^2 + 3r^2 + 2Rr}{4(R^2 + r^2 + Rr)}\right]$$

Thus the initial transverse angular velocity $\omega_0$ can be written as

$$\omega_0 = \frac{v_0 \cos\alpha \sin\left[\arctan\left(\frac{L_c}{r}\sin\alpha\right)\right]}{L_c} \tag{3}$$

and $\omega_1$ can be written as

$$\omega_1 = \frac{v_0\cos\theta - v_{c0}}{L_c} \tag{4}$$

Substituting Eq. (2) into Eq. (4), $\omega_1$ can be written as

$$\omega_1 = \frac{v_0 \cos\left[\arctan\left(\frac{L_c}{r}\sin\alpha\right)\right] - v_{c0}}{r} \tag{5}$$

## 3. Elastic dynamic equations of profiled rod

### 3.1. Assumptions

According to Refs. [9,10], we take the following assumptions.

1) Rod bending due to detonation is not taken into account. The profiled rod is considered as elastic rod, which accords with the assumptions of Euler–Bernoulli beam belonging to variable cross-section Euler–Bernoulli beam.
2) Gravity is not taken into account, and the effect on acceleration of gravity is ignored.
3) The fixed-axis rotation of the profiled rod has occurs in the initial state.
4) The effects on tip resistance and viscous friction of the rod are neglected, and the aerodynamic drag is perpendicular to the axis of the profiled rod.
5) The elastic deformation is presumed not to bring about the changes in aerodynamic drag in order to resolve the corresponding vibration used rod aerodynamic force as external-exciting force. The elastic deformation is loaded to the elastic rod, and then the aerodynamic drag can be achieved. Ultimately, the flight trajectory of the rod is obtained by repeating above-mentioned process.

### 3.2. Establishment of elastic dynamic equations

The flight motion of the profiled rod is made up of the fixed-axis rotation about the center of mass and the translation about the center of mass, as shown in Figs. 3 and 4. The differential equation for transverse vibration on the rotational plane and translation plane and the differential equation for longitudinal vibration on the translation plane can be set up by Newton's second law of motion combined with the theory of Euler–Bernoulli beam. The elastic dynamic equations can be written as

$$\frac{\partial u(x,t)}{\partial x}\left(EA(x)\frac{\partial u(x,t)}{\partial x}\mathrm{d}x\right)-\rho A(x)\frac{\partial^2 u(x,t)}{\partial t^2}=-\rho A(x)x\omega_0^2 \tag{6}$$

$$\frac{\partial^2 v(x,t)}{\partial x^2}\left(EI(x)\frac{\partial^2 v(x,t)}{\partial x^2}\right)+\rho A(x)\frac{\partial^2 v(x,t)}{\partial t^2}=-q(x,t) \tag{7}$$

$$\frac{\partial^2 w(x,t)}{\partial x^2}\left(EI(x)\frac{\partial^2 w(x,t)}{\partial x^2}\right)+\rho A(x)\frac{\partial^2 w(x,t)}{\partial t^2}=-q_z(x,t) \tag{8}$$

where $u(x,t)$, $v(x,t)$ are the longitudinal and transverse displacements deviating from the origin of the cross-section $x$ at the moment $t$, respectively; $\rho$ is the density of rod; $A(x)$ is the area of the cross-section; $E$ is Young's modulus; $\omega_0$ is the angular velocity of the rod on rotational plane; $q(x,t)$ is the transverse force (aerodynamic drag) of the rod in a unit length on rotation plane; $I(x)$ is the second moment of area with respect to the neutral axis of the cross-section; $w(x,t)$ is the transverse displacement from the origin of the cross-section $x$ at the moment $t$; and $q(x,t)$ is the transverse force (aerodynamic drag) of the rod in a unit length on translation plane.

### 3.3. Semi-analytical method for calculating transverse vibration characteristics of profiled rod

Eqs. (6)–(8) are used to calculate the force vibration of variable cross-section beam, and the vibration theory is used to acquire $u(x,t)$, $v(x,t)$, $w(x,t)$ [11,12].

Take an example of equation for transverse vibration of profiled rod on the rotational plane. Obviously, Eq. (7) is the force vibration about lateral deformation $v(x,t)$ under the force $q(x,t)$. Based on the theory of Euler–Bernoulli beam, the equation for free vibration of the rod with length of $L$, direction of transverse vibration is

$$\frac{\partial^2 v(x,t)}{\partial x^2}\left(EI(x)\frac{\partial^2 v(x,t)}{\partial x^2}\right)+\rho A(x)\frac{\partial^2 v(x,t)}{\partial t^2}=0 \tag{9}$$

where $v(x,t)$ is the function of deformation; $EI(x)$ and $\rho A(x)$ are the transverse bending stiffness and linear density, respectively.

The profiled rod is divided into a finite number of homogeneous stepped beams with constant cross-section by using the finite element method, both the ends of the beam are called node. Therefore, the profiled rod is changed into an aggregation with finite beam elements interconnected at the node, and the deflection of arbitrary element can be described as linear combinations composed by nodal displacement so that we can obtain the approximate solution of the profiled rod while the segments are more enough. The profiled rod in Fig. 5 is divided into a finite number of homogeneous stepped beams with constant cross-section by using the finite element method, as shown in Fig. 6.

Introduce $(EI)_i$ and $(\rho A)_i$ as follows

$$\left.\begin{aligned}(EI)_i&=\frac{1}{l_i}\int_{x_{i+1}}^{x_i}EI(x)\mathrm{d}x\\(\rho A)_i&=\frac{1}{l_i}\int_{x_{i+1}}^{x_i}\rho A(x)\end{aligned}\right\} \tag{10}$$

where $l_i$ is the length of the $i$th section beam; $(EI)_i$ is the equivalent longitudinal bending stiffness; and $(\rho A)_i$ is the equivalent linear density.

The modal function of the $i$th section beam can be obtained on the basis of vibration mode for constant cross-section as

$$Y_i(x)=A_i\sin X_i+B_i\cos X_i+C_i\sinh X_i+D_i\cosh X_i \tag{11}$$

where $X_i(x)=\beta_i(x-x_{i-1})$, $x_{i-1}\le x\le x_i$, $(i=1,2,\ldots,\mathrm{N})$, $x_0=0$; $A_i$, $B_i$, $C_i$, $D_i$ are the undefined coefficients of the $i$th section beam; besides,

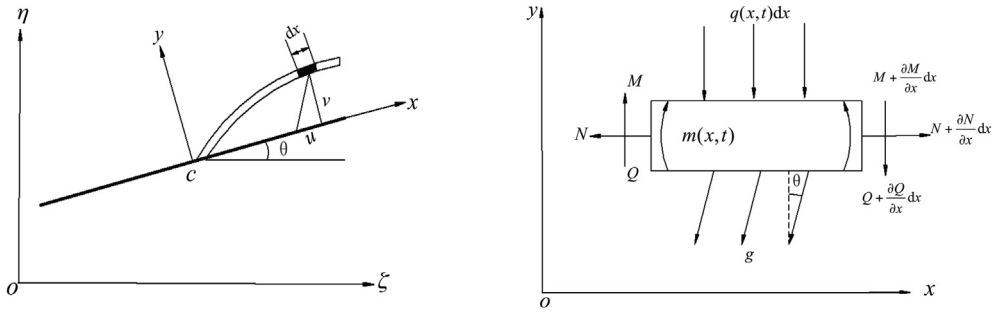


(a) Rotation coordinate system and element displacement (b) Element force analysis with rotation

Fig. 3. Rotation motion of profiled rod.

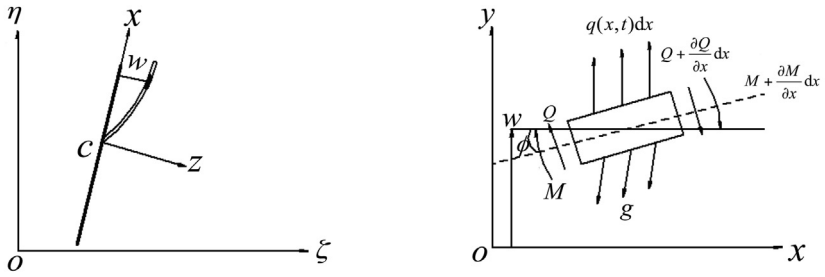


(a) Translation coordinate system and element displacement (b) Element force analysis with translation

Fig. 4. Translation motion of profiled rod.

$$\beta_i^4 = \frac{(\rho A)_i}{(EI)_i}\omega_i^2 \tag{12}$$

where $\omega$ is the natural lateral vibration frequency of variable cross-section beam.

$$Y_{i+1}(x) = A_{i+1}\sin X_{i+1} + B_{i+1}\cos X_{i+1} + C_{i+1}\sinh X_{i+1} + D_{i+1}\cosh X_{i+1} \tag{13}$$

Under the continuous conditions of deflection, rotation, moment and shear force at the point of $x_i$ between the $i$th section beam and the $(i+1)$th section beam. We can acquire the relationships as follows

$$\left.\begin{aligned} &Y_{i+1}(x_i) = Y_i(x_i)\\ &Y'_{i+1}(x_i) = Y''_i(x_i)\\ &(EI)_{i+1}Y''_{i+1}(x_i) = (EI)_i Y''_i(x_i)\\ &\left[(EI)_{i+1}Y''_{i+1}(x_i)\right]' = \left[(EI)_i Y''_i(x_i)\right]' \end{aligned}\right\} \tag{14}$$

Substituting Eqs. (11) and (13) into Eq. (14), we have

$$\boldsymbol{A}_{(i+1)} = \boldsymbol{Z}_{(i)}\boldsymbol{A}_{(i)} \tag{15}$$

and

$$\boldsymbol{A}_{(i)} = [A_i \quad B_i \quad C_i \quad D_i]^{\mathrm{T}},\ \boldsymbol{A}_{(i+1)} = [A_{i+1} \quad B_{i+1} \quad C_{i+1} \quad D_{i+1}]^{\mathrm{T}} \tag{16}$$

$\boldsymbol{Z}_{(i)}$ can be written as

$$\boldsymbol{Z}_{(i)} = \begin{bmatrix} m_1 n_1 & -m_1 n_1 & -m_2 n_4 & -m_2 n_3 \\ m_3 n_1 & m_3 n_1 & -m_4 n_3 & -m_4 n_4 \\ -m_2 n_2 & m_2 n_1 & m_1 n_4 & m_1 n_3 \\ -m_4 n_1 & -m_4 n_2 & m_3 n_3 & m_3 n_4 \end{bmatrix} \tag{17}$$

where

$$m_{1,2} = \beta_i(p \pm 1)/(2\beta_{i+1})$$

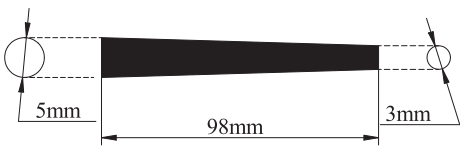


Fig. 5. Variable circular cross-section beam.

$$m_{3,4} = (p \pm 1)/2$$

$$p = (EI)_i\beta_i^2/\left[(EI)_{i+1}\beta_{i+1}^2\right]$$

$$n_1 = \sin(\beta_i l_i)$$

$$n_2 = \cos(\beta_i l_i)$$

$$n_3 = \sinh(\beta_i l_i)$$

$$n_4 = \cosh(\beta_i l_i)$$

These recursive relations are used to establish a new algorithm for $A_{(1)}$ and $A_{(N)}$

$$\boldsymbol{A}_{(N)} = \boldsymbol{Z}\boldsymbol{A}_{(1)} = \boldsymbol{Z}_{(N-2)}\boldsymbol{Z}_{(N-2)}\ldots\boldsymbol{Z}_{(2)}\boldsymbol{Z}_{(1)}\boldsymbol{A}_{(1)} \tag{18}$$

The relationship of undetermined coefficient between the first equivalent beam and the $N$th equivalent beam is built by matrix $\boldsymbol{Z}$ where all the elements are the function of natural frequency. Consequently, the solution of modal function can be obtained from Eqs. (11) and (18) by solving the natural frequency with four boundaries at both ends of the beam.

After the detonation, the profiled rods fly rapidly in parallel to the axes of the warhead, as the result of the geometric asymmetry, the motion performances of the rods are complicated. The different flight attitudes of the rods were demonstrated in forward flight. Two boundary conditions were presented to illustrate the aeroelastic response by terms of different flight attitudes.

### 3.4. Boundary conditions

#### 3.4.1. Clamped–clamped beam

For instance, the case where the beam is clamped at both its ends is considered, as shown in Fig. 7. The governing boundary conditions are as follows

$$Y_1(0) = 0, \quad (EI)_1 Y'_1(0) = 0 \tag{19}$$

$$Y_N(L) = 0, \quad (EI)_N Y'_N(L) = 0 \tag{20}$$

Eqs. (19) and (20) are rewritten as the form of matrix

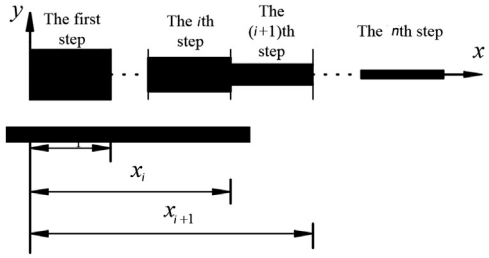


Fig. 6. Stepped beam with $N$ segments.

$$\boldsymbol{\Gamma A}(1)=0 \tag{21}$$

where

$$\boldsymbol{\Gamma}=\left[\boldsymbol{\Gamma}_1^{\mathrm{T}}\ \ \boldsymbol{\Gamma}_2^{\mathrm{T}}\ \ \boldsymbol{\Gamma}_3^{\mathrm{T}}\ \ \boldsymbol{\Gamma}_4^{\mathrm{T}}\right]^{\mathrm{T}},\ \boldsymbol{\Gamma}_1=[1\ \ 0\ \ 1\ \ 0],\ \boldsymbol{\Gamma}_2=[0\ \ 1\ \ 0\ \ 1]$$

$$\boldsymbol{\Gamma}_3=[\sin l_{i+1}\ \ \cos l_{i+1}\ \ \sinh l_{i+1}\ \ \cosh l_{i+1}]Z$$

$$\boldsymbol{\Gamma}_4=[\cos l_{i+1}\ \ -\sin l_{i+1}\ \ \cosh l_{i+1}\ \ \sinh l_{i+1}]Z$$

The determinants of coefficient matrix must be equal to zero if Eq. (16) has a solution.

$$\det\boldsymbol{\Gamma}=0 \tag{22}$$

When characteristic Eq. (22) is a nonlinear function $\omega$, it can be solved by Newton–Raphson iteration extensions to obtain the natural lateral vibration frequency in responding boundary conditions. Then $\omega$ is substituted into Eqs. (11) and (15) to obtain the principal mode of the beam. Furthermore, the elastic deformation can be also solved by a mode superposition method [13,14].

*3.4.2. Free-clamped beam*

Here, the differences between this condition, as shown in Fig. 8, and the above-mentioned computation are the boundary conditions.

$$Y_1(0)=0\ \ (EI)_1Y_1'(0)=0 \tag{23}$$

$$Y_N''(L)=0,\ \ (EI)_NY_N''{}'(L)=0 \tag{24}$$

where

$$\boldsymbol{\Gamma}=\left[\boldsymbol{\Gamma}_1^{\mathrm{T}}\ \ \boldsymbol{\Gamma}_2^{\mathrm{T}}\ \ \boldsymbol{\Gamma}_3^{\mathrm{T}}\ \ \boldsymbol{\Gamma}_4^{\mathrm{T}}\right]^{\mathrm{T}},\ \boldsymbol{\Gamma}_1=[1\ \ 0\ \ 1\ \ 0],\ \boldsymbol{\Gamma}_2=[0\ \ 1\ \ 0\ \ 1]$$

$$\boldsymbol{\Gamma}_3=[-\sin X_{i+1}\ \ -\cos X_{i+1}\ \ \sinh X_{i+1}\ \ \cosh X_{i+1}]Z$$

$$\boldsymbol{\Gamma}_4=[-\cos X_{i+1}\ \ -\sin X_{i+1}\ \ \cosh X_{i+1}\ \ \sinh X_{i+1}]Z$$

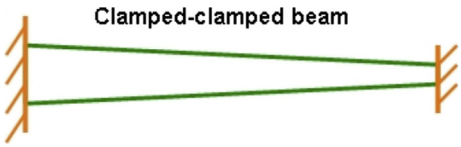


Fig. 7. Clamped–clamper beam.

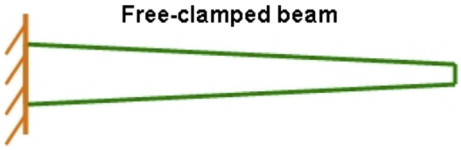


Fig. 8. Free-clamper beam.

## 4. Numerical simulation method

A two-way coupling approach is proposed in order to solve the static aeroelastic problem of a profiled rod to conduct this static aeroelastic analysis, ANSYS Workbench multi-physics coupling platform, which includes fluid, structural solvers and coupling module, namely FLUENT, ANSYS Mechanical and System coupling, is used to solve the displacements associated with the aerodynamic pressure loading and find out the static aeroelastic behavior of this variable cross-section rod. CFD grid is deformed to obtain the aerodynamic solutions of the deformed geometry using dynamic mesh which is called diffusion-based smoothing method. For the structural analysis, the ANSYS Mechanical inertia relief option [15,16], which is based on d'Alembert principle, is used to simulate the unconstrained rockets in flight and makes sure the rocket has no rigid body displacement, is used with the linear elastic solver. The aerodynamic coefficients distribution of the profiled rod and the elastic deformation are calculated and compared with program results. The steps of static aeroelastic calculation are described and the coupling procedure is explained in the following section.

### *4.1. CFD governing equations*

For CFD problems, the direct numerical simulation (DNS) is used to solve the Navier–Stokes (N–S) equations without the turbulent model which needs high speed and large memory computer due to their high nonlinearity and complexity. It is impossible to adopt this method in practical engineering. Decomposing the N–S equations into the RANS equations makes it possible to simulate the engineering fluid dynamic problems.

Reynolds averaged N–S equations (RANS) can be expressed as

$$\frac{\partial\boldsymbol{Q}}{\partial t}+\frac{\partial\boldsymbol{E}}{\partial x}+\frac{\partial\boldsymbol{F}}{\partial y}+\frac{\partial\boldsymbol{G}}{\partial z}=\frac{\partial\boldsymbol{E}_v}{\partial x}+\frac{\partial\boldsymbol{F}_v}{\partial y}+\frac{\partial\boldsymbol{G}_v}{\partial z} \tag{25}$$

where

$$\boldsymbol{Q}=[\rho,\ \rho u,\ \rho v,\ \rho w,\ \rho E]^{\mathrm{T}}$$

$$\boldsymbol{E}=\left[\rho u,\ \rho u^2+p,\ \rho uv,\ \rho uw,\ (\rho E+p)u\right]^{\mathrm{T}}$$

$$\boldsymbol{F}=\left[\rho v,\ \rho vu,\ \rho v^2+p,\ \rho vw,\ (\rho E+p)v\right]^{\mathrm{T}}$$

$$\boldsymbol{G}=\left[\rho w,\ \rho wu,\ \rho wv,\ \rho w^2+p,\ (\rho E+p)w\right]^{\mathrm{T}}$$

$$\boldsymbol{E}_v = \left[0,\ \tau_{xx},\ \tau_{xy},\ \tau_{xz},\ \beta_x\right]^{\mathrm{T}}$$

$$\boldsymbol{F}_v = \left[0,\ \tau_{yx},\ \tau_{yy},\ \tau_{yz},\ \beta_y\right]^{\mathrm{T}}$$

$$\boldsymbol{G}_v = \left[0,\ \tau_{zx},\ \tau_{zy},\ \tau_{zz},\ \beta_z\right]^{\mathrm{T}}$$

where $\rho$ is the fluid density; $u$, $v$, $w$ are the three components of Cartesian coordinate system; $p$ is pressure; and $E$ is total energy of unit mass.

For the closure of above equations, the shear stress transport (SST) k−ω turbulence model developed by Menter [17,18] is used. SST model combines the advantages of standard k−ε and standard k−ω models. $k$ and $\omega$ transport equations can be written as

$$\frac{\mathrm{d}(\rho k)}{\mathrm{d}t} = \tau_{ij}\frac{\partial u_i}{\partial x_j} - \beta^*\rho\omega k + \frac{\partial}{\partial x_j}\left[(\mu + \sigma_k\mu_t)\frac{\partial k}{\partial x_j}\right] \tag{26}$$

$$\begin{aligned}\frac{\mathrm{d}(\rho\omega)}{\mathrm{d}t} =& \frac{\gamma\rho}{\mu_t}\tau_{ij}\frac{\partial u_i}{\partial x_j} - \beta\rho\omega^2 + \frac{\partial}{\partial x_j}\left[(\mu + \sigma_\omega\mu_t)\frac{\partial\omega}{\partial x_j}\right] \\ &+ 2\rho(1-F_1)\sigma_{\omega 2}\frac{1}{\omega}\frac{\partial k}{\partial x_j}\frac{\partial\omega}{\partial x_j}\end{aligned} \tag{27}$$

where $\tau_{ij}$ is shear stress

$$\tau_{ij} = \mu_t\left(\frac{\partial u_i}{\partial x_j} + \frac{\partial u_j}{\partial x_i} - \frac{2}{3}\frac{\partial u_k}{\partial x_k}\delta_{ij}\right) - \frac{2}{3}\rho k\delta_{ij} \tag{28}$$

Blending function$F_1$

$$F_1 = \tan h\left(\arg_1^4\right) \tag{29}$$

where

$$\arg_1 = \min\left[\max\left(\frac{\sqrt{k}}{0.09\omega y}, \frac{500v}{y^2\omega}\right), \frac{4\rho\sigma_{\omega 2}k}{CD_{k\omega}y^2}\right]$$

$$CD_{k\omega} = \max\left(2\rho\sigma_{\omega 2}\frac{1}{\omega}\frac{\partial k}{\partial x_j}\frac{\partial\omega}{\partial x_j},\ 10^{-20}\right)$$

The eddy viscosity is defined as

$$\mu_t = \frac{\rho\alpha_1 k}{\max(\alpha_1\omega, \Omega F_2)} \tag{30}$$

where $\Omega$ is the absolute value of the vorticity. $F_2$ is given by

$$F_2 = \tan h\left(\arg_2^2\right) \tag{31}$$

where

$$\arg_2 = \max\left(\frac{2\sqrt{k}}{0.09\omega y}, \frac{500\mu}{\rho y^2\omega}\right)$$

The constant$\phi$ of SST model are calculated from the constants $\phi_1$,$\phi_2$ as follows

$$\phi = F_1\phi_1 + (1-F_1)\phi_2 \tag{32}$$

where set 1($\phi_1$) is the constant of $k-\omega$ model, and set 2($\phi_2$) is the constant of $k-\varepsilon$ model. The constants of set 1($\phi_1$) are

$$\sigma_{k1} = 0.5,\ \sigma_{\omega 1} = 0.5,\ \beta_1 = 0.075,\ \beta^* = 0.09,\ \kappa = 0.41,$$
$$\gamma_1 = \left(\beta_1/\beta^*\right) - \left(\sigma_{\omega 1}\kappa^2\Big/\sqrt{\beta^*}\right)$$

The constants of set 2($\phi_2$) are

$$\sigma_{k2} = 1.0,\ \sigma_{\omega 1} = 0.856,\ \beta_2 = 0.0828,\ \beta^* = 0.09,\ \kappa = 0.41,$$
$$\gamma_2 = \left(\beta_2/\beta^*\right) - \left(\sigma_{\omega 2}\kappa^2\Big/\sqrt{\beta^*}\right)$$

All other parameters are given in Ref. [18].

Density, velocity, pressure, etc. at every grid node could be computed by solving the above equations. Then, normal, axial, lift, drag, pitching moment and center of the pressure coefficients can be obtained by the following equations, respectively

$$\begin{cases} C_{\mathrm{N}} = N/q_\infty S \\ C_{\mathrm{A}} = A/q_\infty S \\ C_{\mathrm{L}} = C_{\mathrm{N}}\times\cos\alpha - C_{\mathrm{A}}\times\sin\alpha \\ C_{\mathrm{D}} = C_{\mathrm{N}}\times\sin\alpha + C_{\mathrm{A}}\times\cos\alpha \\ C_{\mathrm{m}} = pitching\quad moment/q_\infty Sl \\ x_{\mathrm{cp}} = x_{\mathrm{cg}} - (C_{\mathrm{m}}/C_{\mathrm{N}}) \end{cases} \tag{33}$$

where $q_\infty$, $\alpha$, $S$, $x_{\mathrm{cp}}$ and $x_{\mathrm{cg}}$ are the dynamic pressure, angle of attack, reference area, center of pressure location and center of gravity location, respectively; $l$ is the length of rod.

### 4.2. Static structure analysis equations

A static structural analysis determines the displacements, stresses, strains, and forces in the structures or components caused by loads that do not induce significant inertia and damping effects. Steady loading and response conditions are assumed, that is, the loads and the structure's response vary slowly with respect to time. This is an isotropic linear elastic problem. The static structure analysis equation can be written as

$$[\boldsymbol{K}]\{\boldsymbol{\delta}\} = \{\boldsymbol{F}\} \tag{34}$$

where $[\boldsymbol{K}]$ is stiffness matrix; $\{\delta\}$ is displacement vector; and $\{\boldsymbol{F}\}$ is force vector.

For these linear elastic structural mechanics problems, $K$ is a constant, and the aerodynamic force $F$ is calculated by CFD code. Then the deformation $\delta$ can be obtained.

### 4.3. Coupling boundary conditions

In the fluid-structure interaction work, there is a boundary where the interactions of fluid and structural domains occur at this boundary or interface. Deformation compatibility and force equilibrium conditions should be satisfied on the fluid-structure coupling interface [19]:

$$\begin{cases} d_f = d_s \\ n \cdot \tau_f = n \cdot \tau_s \\ q_f = q_s \\ T_f = T_s \end{cases} \quad (35)$$

where $d$, $q$, $T$, and $\tau$ are displacement, heat flux, temperature and stress field on the fluid-structure coupling interface, respectively; $n$ is the normal direction of interface, and subscripts $f$ and $s$ are the fluid and the solid, respectively.

## 5. Discussions on the comparison of two methods

The profiled rod is shown in Fig. 5. Here the initial deformation caused by detonation is not considered, the constraint conditions can be used as clamped–clamped based on the initial conditions, and the aerodynamic load and the aerodynamic coefficient obtained by using quasi-steady aerodynamics are 890 N and 1.16, respectively. The aeroelastic deformation can be solved by the equations for elastic vibration. Maximum deformation was obtained at the left side (where $D = 3$ mm) of the rod at 39 mm from the origin.

In order to test the accuracy of the numerical results, we have developed a special low-cost numerical method, computational fluid dynamic finite element method (CFD/FEM), useful for studies, based on the actual model.

The numerical results are summarized in Fig. 9. As shown in Fig. 9, the maximum elastic deformation of the numerical results is 0.9 mm, the maximum elastic deformation of the CFD results is 0.7 mm, and the maximum elastic deformation appears at the left side (where $D = 3$ mm) of the rod at 39 mm from the origin. This gave a good agreement with results on the undeformed profiled rod. The calculated aeroelastic deformation is substituted into Eq. (12) to solve the aerodynamics and the drag aerodynamic coefficient. The drag aerodynamic coefficient is 1.16 that indicates the elastic deformation almost has no influence on the flight performance.

It is well known that the rods, which are explosively deployed from its warhead mechanism, generate obvious plastic deformation (Fig. 10). Therefore, the discussion on the flight attitude of profiled rod should be taken account for initial deformation generated from previous explosion wave impacts.

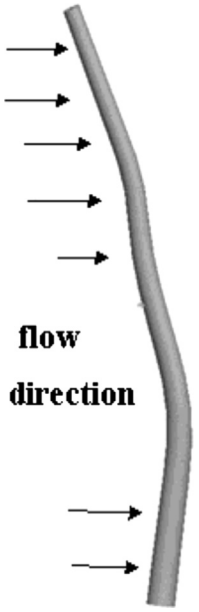


Fig. 10. Profiled rod after detonation.

Fig. 11 shows the elastic deformation of deformed rod. Here, it is noticed that the maximum elastic deformation of the undeformed profiled rod is significantly higher than that of the deformed profiled rod. It is considered that this difference is due to the initial deformation of the profiled rod. Namely, when the initial deformation of unreformed rod is considered, the results will be consistent. On the other hand, the relative elastic deformation is so small that we can neglect its impact on the flight performance. Therefore, the semi-analytical method can be used to calculate the vibration characteristics of variable cross-section beam, which solves the elastic deformation for elastic dynamic equations of profiled rod based on the theory of Euler–Bernoulli beam model. Moreover, the rigid body motion can be used to describe the motion of the profiled rod flying against air resistance at high velocity.

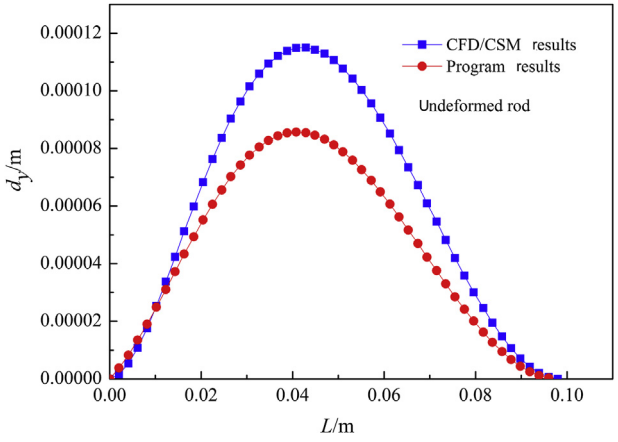


Fig. 9. The maximum deformation of undeformed profiled rod with transverse vibration.

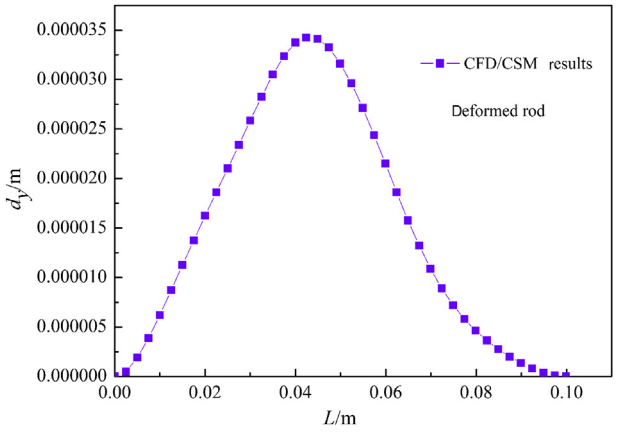


Fig. 11. Deformation of deformed rod with bending vibration.

## 6. Conclusions

A new conceptual KER warhead named profiled rod warhead was proposed firstly. The design principle of profiled rod was described and the deployment velocity of rod was obtained.

Regarding the profiled rod as Euler−Bernoulli beam model, the elastic dynamic equations of the profiled rod were established to analyze the aeroelastic effect of rod flying at high velocity, and semi-analytical method was used to calculate the aeroelastic deformation.

Besides, some efforts are applied to test the numerical results by using CFD/FEM. A satisfactory agreement is obtained by comparing the numerical results and CFD/FEM results.

The proposed model has been proven to be able to simulate the actual phenomena that the deformed rod after detonation flying at high velocity. The model can be modified for the parametric studies of intricate design change details, such as diameter or length of profiled rod, initial velocity of detonation or other similar changes in the design of the profiled rod warhead. In addition, the model built in this paper may be the foundation for the research on flight performance of the profiled rod deployed by detonation, and provides a theoretical basis of describing the aerodynamic and the bomb fall characteristics. Moreover, the model may give great convenience to the design of the profiled rod warhead.

## References

[1] Lloyd Richard M, Sebeny JL. Physics of kinetic energy rod warheads against TBM submunition payloads. AIAA 1999:1−20.
[2] Lloyd Richard M, Sebeny JL. Novel penetrator study for defeat of ballistic missile payloads. Int J Impact Eng 2006;33:380−9.
[3] Richard M. Lloyd. Kinetic energy rod warhead with optimal penetrator [P]. US, 6,779,462 B2, 2004.
[4] Richard M. Lloyd. Warhead with aligned projectiles [P]. WO, 03/042624 A2, 2003.
[5] Richard M. Lloyd. Kinetic energy rod warhead with lower deployment angles [P]. WO, 05/022074 A2, 2005.
[6] Qian JP, Cao B, Shen PH. Overview of ammunition. Beijing: National Defence Industry Press; 2004. p. 267−70 [in Chinese].
[7] Sun CJ, Lu ZH, Lu YG, Wen Y, Sun Y. Motion analysis of controllable rotation discrete rod. Explos Shock Waves 2008;28(4):379−83 [in Chinese].
[8] Liu ZJ, Xiao C, Wang QH. The design analysis on the controllable rotation discrete rod. J Explos 2000;23(4):48−50 [in Chinese].
[9] Cai ZB. Dynamic characteristics of high-speed flight discrete rod and penetration effect to the target. Ph.D. Thesis. Nanjing: Nanjing University of Science and Technology; 2005 [in Chinese].
[10] Wang LM. An analysis on the flexibility in flight of projectiles or rockets having high L/D ratios. Acta Armamentarii 2000;21(2):109−11 [in Chinese].
[11] Cui C, Jiang H, li YH. Semi-analytical method for calculating vibration characteristics of variable cross-section beam. J Vib Shock 2012;31(14):85−8 [in Chinese].
[12] Ni ZH. Vibration mechanics. Xi'an: Xi'an Jiaotong University Press; 1989 [in Chinese].
[13] Shabana AA. Resonance conditions and deformable body coordinate systems. J Sound Vib 1996;192(1):389−98.
[14] Escalona JL, Valverde J, Mayo J, Dominguez. Reference motion in deformable bodies under rigid body motion and vibration. Part II: evaluation of the coefficient of restitution for impacts. J Sound Vib 2003;264:1057−72.
[15] Lin L. A study of inertia relief analysis. In: 52nd AIAA/ASME/ASCE/AHS/ASC structures, structural dynamics and materials conference, Denver, Colorado; 2011. AIAA2011−2002.
[16] Chen ZT, Sun Q. Applications of inertia relief method in aircraft static aero-elasticity. Flight Dyn 2008;26(5):71−4 [in Chinese].
[17] Menter FR. Zonal two equation k−ω turbulence models for aerodynamic flows. In: 24th fluid dynamics conference, Orlando, Florida; 1993. p. 1−21. AIAA 93-2906.
[18] Menter FR. Two-equation eddy-viscosity models for engineering applications. AIAA 1994;32(8):1598−605.
[19] Han ZZ. FLUENT-examples and analysis of flow filed calculation of engineering. Beijing: Beijing Institute of Technology Press; 2009. p. 13−9 [in Chinese].